The mechanical properties and the deformation microstructures of the C15 Laves phase Cr2Nb at high temperatures

Kazantzis, A. V.; Aindow, M.; Jones, I. P.; Triantafyllidis, G. K.; De Hosson, J.T.M.

Published in:
Acta Materialia

DOI:
10.1016/j.actamat.2006.10.048

Publication date:
2007

Available online at www.sciencedirect.com
ScienceDirect
Acta Materialia 55 (2007) 1873–1884
Acta MATERIALIA
www.actamat-journals.com

The mechanical properties and the deformation microstructures of the C15 Laves phase Cr_2Nb at high temperatures

A.V. Kazantzis [a,*], M. Aindow [b], I.P. Jones [c], G.K. Triantafyllidis [d], J.Th.M. De Hosson [a]

[a] Department of Applied Physics, Materials Science Centre and Netherlands Institute for Metals Research, University of Groningen, Nijenborgh 4, 9747 AG Groningen, The Netherlands
[b] Department of Metallurgy and Materials Engineering, Institute of Materials Science, The University of Connecticut, 97 North Eagleville Road, Storrs, CT 06269-3136, USA
[c] School of Metallurgy and Materials & Interdisciplinary Research Centre in Materials for High Performance Applications, Faculty of Engineering, The University of Birmingham, B15 2TT Edgbaston, Birmingham, UK
[d] Aristotle University of Thessaloniki, Faculty of Engineering, Chemical Engineering Department, Laboratory of Materials Technology, Region of Central Macedonia 540 24, Greece

Received 21 August 2006; received in revised form 12 October 2006; accepted 14 October 2006
Available online 3 January 2007

Abstract

Compression tests between 1250 and 1550 °C and 10^{-5} and 5×10^{-3} s^{-1} and transmission electron microscopy have been employed to investigate the high temperature mechanical properties and the deformation mechanisms of the C15 Cr_2Nb Laves phase. The stress-peaks in the compression curves during yielding were explained using a mechanism similar to strain aging combined with a low initial density of mobile dislocations. The primary deformation mechanism is slip by extended dislocations with Burgers vector $1/2\langle 1\,1\,0\rangle$, whereas twinning is more frequent at 10^{-4} s^{-1}. Schmid factor analysis indicated that twinning is more probable in grains oriented so as to have two co-planar twinning systems with high and comparable resolved shear stresses. Twinning produced very anisotropic microstructures. This may be due to synchroshear: a self-pinning mechanism which requires co-operative motion of zonal dislocations.

Keywords: Laves phases; Mechanical properties testing; Compression test; Transmission electron microscopy (TEM); High temperature deformation

1. Introduction

The intermetallic compound Cr_2Nb has been considered as a potential material for high temperature structural applications because it exhibits oxidation resistance superior to that of conventional Ni-based superalloys and its density is relatively low (7.7 g/cm^3) [1,2]. It exhibits a relatively wide single-phase field and since Laves phases comprise one of the largest intermetallic groups, its poor low temperature ductility may well be improved by alloying additions. Cr_2Nb exhibits the cubic C15 ($MgCu_2$-type) structure below ~1600 °C and the hexagonal C14 ($MgZn_2$-type) structure between this temperature and its melting point (between 1730 and 1770 °C) [3,4]. Both crystal structures are topologically close-packed (TCP), with tetrahedra of the major element (Cr) placed within face-centred cubic or hexagonal close-packed arrangements of the minority element (Nb). In the usual notation for elemental close-packed structures, the $\{1\,1\,1\}$ or $(0\,0\,0\,1)$ planes are close-packed layers, denoted **A**, **B** and **C**, but for Laves phases each plane consists of four adjacent atomic nets. Three of these are triangulated "3^6" layers, and form a sandwich which is firmly fitted in the holes of an underlying kagomé "3636" net. Along the $\langle 1\,1\,1\rangle$ the C15 structure has a stacking sequence ... **ABCABC** ..., analogous to that of the fcc close-packed structures, whereas for the C14 structure the $(0\,0\,0\,1)$ sequence is the ... **ABAB** ... of the hcp structure. In the Laves phases, however, a more faithful description would include the individual atomic nets, where Roman

* Corresponding author. Tel.: +31 50 3634890; fax: +31 50 3634881.
E-mail address: avkazantzis@hol.gr (A.V. Kazantzis).

1359-6454/$30.00
doi:10.1016/j.actamat.2006.10.048

characters represent the Cr nets (capitals for the kagomé nets) and Greek characters, those formed by the large Nb atoms (e.g. **A**: Aαcβ) [5]. Hence the precise {1 1 1} sequence for the C15 structure becomes

$$\begin{array}{cccccccc} \ldots & \mathbf{A} & \mathbf{B} & \mathbf{C} & \mathbf{A} & \mathbf{B} & \mathbf{C} & \ldots \\ \ldots & (\mathrm{A}\alpha\mathrm{c}\beta)\text{–}(\mathrm{B}\beta\mathrm{a}\gamma)\text{–}(\mathrm{C}\gamma\mathrm{b}\alpha)\text{–}(\mathrm{A}\alpha\mathrm{c}\beta)\text{–}(\mathrm{B}\beta\mathrm{a}\gamma)\text{–}(\mathrm{C}\gamma\mathrm{b}\alpha) & & & & & & \ldots, \end{array}$$

whereas the (0 0 0 1) sequence of the C14 structure is similarly described by:

$$\begin{array}{ccccccc} \ldots & \mathbf{A} & \mathbf{B}' & \mathbf{A} & \mathbf{B}' & \mathbf{A} & \ldots \\ \ldots & (\mathrm{A}\alpha c\beta) - (\mathrm{B}\beta c\alpha) - (\mathrm{A}\alpha c\beta) - (\mathrm{B}\beta ca) - (\mathrm{A}\alpha c\beta) & & & & & \ldots \end{array}$$

Note that the stacking of the atomic nets in a plain quadruple layer (e.g. **B**: Bβaγ) is markedly different from that in a primed layer (e.g. **B′**: Bβcα). These two variants are twin-related to each other and influence the layer succession in the Laves phase structures since only stackings of the type **A** (Aαcβ) → **B** (Bβaγ), or **A′** (Aαbγ) → **C** (Cγbα) are allowed. The different sizes of the atomic species that form binary Laves phases result in complex polyhedra with high coordination numbers (CN) (i.e., icosahedra with CN 12 and Friauf icosioctahedra with CN 16). These are more intricate than the cubo-octahedral coordinations in the elemental close-packed configurations; they produce crystal structures with very small tetrahedral interstices and atomic densities that are higher than those of the elemental fcc and hcp metals.

Ordered intermetallics such as the C14/C15 Cr_2Nb are inherently strong; they maintain their strength at high temperatures and exhibit high creep resistance [6]. In addition, the C15 structure is especially attractive due to the fcc Bravais lattice, which suggests the existence of sufficient independent slip and/or twinning systems for general plastic deformation. As a single phase alloy, however, Cr_2Nb has a ductile to brittle transition temperature (DBTT) of ~1250 °C and exhibits poor damage tolerance at room temperature [7]. It must be emphasized that, even though the original concept of DBTT is based on notched Charpy impact tests, it is somewhat misused throughout the present work. Since, regrettably, there is not an analogous term to indicate the lowest temperature where compression specimens can be plastically deformed, this term will still be used henceforth for that purpose.

Most Laves phases are generally brittle up to high homologous temperatures, even as single crystals [8,9]. It has been established, however, that the high DBTT of the C15 Cr_2Nb is not associated with strong directional bonds since it is only a weakly covalent compound [10], but rather with the complexity of the crystal structure, which is also responsible for the alloy's good high temperature strength. The C15 Cr_2Nb has a highly symmetrical cubic unit cell with 24 atoms whose elemental radius ratio is well below the ideal ($R_{Nb}/R_{Cr} = 1.15 < 1.225$) and they form a tightly packed structure where dislocations are expected to move with substantial difficulty. They encounter high Peierls forces and require complex atomic motions [11,12]. Any dislocation motion is presumably accompanied by complex dissociations and interactions, producing defect configurations with large Burgers vectors, high strain energy and, therefore, Cr_2Nb is ductile only at high temperatures where thermal activation is significant.

Electron microscopy studies of the deformation mechanisms, however, showed that the microstructure was dominated by conventional perfect dislocations with Burgers vectors 1/2⟨1 1 0⟩, which were dissociated into 1/6⟨1 1 2⟩ Shockley partials as might be expected from crystals with fcc lattices [13]. Even though twins were repeatedly observed, especially at low temperatures above the DBTT, their formation was attributed to dynamic recrystallisation, largely because of the presence of stress-peaks in the deformation curves that were followed by softening prior to the establishment of steady-state flow. For most Laves phases formed between transition metals, however, mechanical twinning is considered as the primary deformation mechanism [14–16]. Clearly, there is a need for a better understanding of the deformation behaviour of Cr_2Nb, if this alloy is ever to be used for engineering components for high temperature service.

In this paper we present a full account of the mechanical properties and the deformation mechanisms of single-phase Cr_2Nb, deformed in compression at temperatures between its DBTT and 1550 °C (i.e., below the C14/C15 transformation temperature) and strain rates between 10^{-5} and $5 \times 10^{-3}\ s^{-1}$. By employing transmission electron microscopy (TEM), it was possible to correlate the macroscopic mechanical response of the polycrystalline alloy with the deformation microstructures observed at various testing conditions and to rationalise our results in terms of the current models of deformation in Laves phases.

2. Experimental procedure

Elemental starting materials (Cr and Nb with purity 99.5% and 99.9%, supplied by Johnson Matthey and Aldrich, respectively) were used to prepare a 500 g ingot of nominally stoichiometric Cr_2Nb, by transferred-arc plasma melting in a Retech plasma melting facility under a slight over-pressure of high purity Ar. The ingot was remelted five times, turning before each remelt, to promote homogeneity. It was then sectioned using an SiC cutting wheel into specimens with approximate dimensions $1 \times 1 \times 4$ cm, which were subsequently cleaned and surface smoothed by conventional grinding and polishing methods. These were homogenised at 1400 °C for 2 days in an Ar atmosphere. The heating/cooling rate was 0.1 °C s^{-1}, i.e., sufficiently low as to result in a final material with low residual stresses. X-ray diffraction (XRD) was performed on powder prepared from the homogenised alloy using a Philips PW1050/25 diffractometer. Specimens with approximate dimensions $1.5 \times 1.5 \times 2.5$ mm were prepared from the homogenised material by electrodischarge machining (EDM), surface grinding and polishing in order to ensure the absence of cracks and voids. These were mechanically

compressed in an Instron 5100 frame equipped with W-mesh heating elements within a water-cooled stainless steel vacuum chamber. The chamber was evacuated to 10^{-7} mbar and the Cr_2Nb specimens were uniaxially compressed to a nominal strain of 5% at temperatures, T, between 1250 and 1550 °C and at strain rates, $\dot{\varepsilon}$, varying between 10^{-5} and $5 \times 10^{-3}\ s^{-1}$. Following the completion of the tests, half of the specimens were allowed to cool to 1150 °C before unloading so as to retain the post-mortem deformation microstructure, whereas for the other half, the load was released prior to cooling to promote recovery. For all testing conditions, the compliance of the compression facility was recorded and was removed from the stress–strain curves of Cr_2Nb. If the specimens were seen to have deflected after compression they were excluded from further analysis and their stress–strain curves were not taken into account. Energy dispersive spectrometry (EDS), in a JEOL-840A microprobe analyser, was used to determine the composition of Cr_2Nb specimens prepared before and after deformation by standard grinding and polishing techniques. Their optical microstructure was recorded after they were electrolytically etched under a voltage of 2 V, in a solution of 10 vol.% HF and 20 vol.% HCl in water, using a stainless steel cathode. Specimens for TEM were prepared by cutting thin slices from the deformed samples using EDM, grinding and polishing to a thickness of 100 μm and Ar^+ ion beam thinning to perforation. The microstructure was observed using a Philips CM20 and a JEOL-4000FX TEM operating at 200 and 400 kV, respectively.

3. Results

3.1. The as-cast and annealed microstructures

The TEM microstructure of the as-cast Cr_2Nb revealed a large number of interpenetrating stacking faults (SFs) with densities approaching $1 \times 10^6\ m^{-1}$, terminating mostly at grain boundaries or extending to the surface of the foil (Fig. 1a). The average dislocation density was low (i.e., $\sim 5 \times 10^5\ m^{-2}$) and diffraction contrast analysis determined that these were $1/6\langle 1\,1\,2\rangle$ type Shockley partials, mostly along the $\langle 1\,1\,0\rangle$ orientation at the boundary if a SF on the $\{1\,1\,1\}$ plane. Growth twins were relatively rare in the as-cast material but their volume fraction increased to ~5% after prolonged heat treatment for 2 days at 1400 °C (Fig. 1b and c). They were observed in sharp contrast having boundaries completely free of dislocation debris and they revealed their characteristic twinned diffraction maxima in the $\langle 1\,1\,0\rangle$ selected area diffraction patterns (SADP). The interpenetrating SFs disappeared almost completely and the dislocation density decreased below $10^5\ m^{-2}$. The optical micrograph of the annealed microstructure (Fig. 1d) shows irregular plate like grains with thickness between 60 and 80 μm and length occasionally exceeding 200 μm, with mostly faceted boundaries and frequently crossed by bands. EDS analysis confirmed that

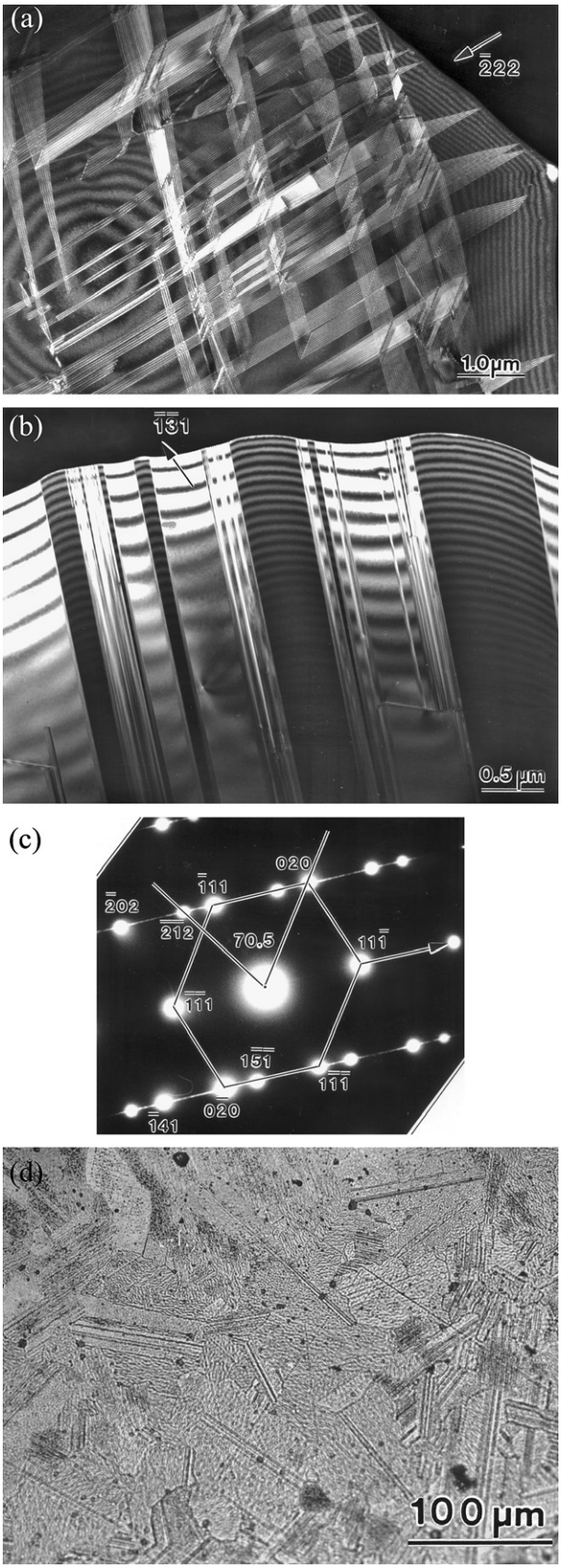

Fig. 1. (a) Interpenetrating SFs in the as-cast Cr_2Nb; (b) annealing twins; (c) $\langle 1\,1\,0\rangle$ twinned SADP; and (d) optical microstructure of the grain morphology after heat treatment at 1400 °C for 2 days.

their composition was 64.1 at.% Cr and 35.9 at.% Nb (±0.7 at.%) and XRD determined that the material was a single phase alloy having the cubic C15 crystal structure and a lattice parameter of $a_0 = 6.9947 \pm 0.0013$ Å.

3.2. Mechanical properties

Plastic deformation was induced at T between 1300 and 1550 °C and at $\dot{\varepsilon}$ between 10^{-5} and 5×10^{-3} s^{-1}. For tests carried out at 1250 °C, plastic deformation was attained only at the lowest strain rate of 10^{-5} s^{-1} (i.e., at the deformation creep regime). At this temperature, the specimens deformed at 5×10^{-5} s^{-1} failed immediately after yielding, whilst at higher strain rates and lower temperatures brittle fracture was always experienced in an explosive manner with complete disintegration of the specimens. Consequently, the temperature of 1250 °C was considered as the DBTT for the material investigated in this study. Fig. 2a–c shows the engineering stress–strain curves for the samples deformed at three representative temperatures (1300, 1400 and 1500 °C) for various strain rates, whereas the stress–strain curves for the compressions at three representative strain rates (10^{-5}, 10^{-4} and 10^{-3} s^{-1}) and various temperatures are shown in Fig. 2d–f. All specimens compressed at $T \leqslant 1400$ °C and at $\dot{\varepsilon} > 1.50 \times 10^{-4}$ s^{-1} revealed stress-peaks prior to macroscopic yielding, which were followed by a substantial softening before the gradual establishment of steady-state flow. The magnitude of these peaks generally decreased with increasing temperature and decreasing strain rate and at $T > 1450$ °C and at $\dot{\varepsilon} < 10^{-4}$ s^{-1} there were no distinct yield points and steady-state flow was established readily during the early stages of deformation, i.e., within 1.5% of nominal strain. Due to these peaks, the use of 0.1% proof stress was considered inadequate to describe accurately the behaviour of Cr_2 Nb at the yield point and thus yield strengths, (σ_y) are quoted instead, obtained at the first deviation yield points indicated by asterisks (*) on the deformation curves. At all temperatures and strain rates, the specimens did not exhibit work hardening and, therefore, flow stresses (σ_f) were measured with substantially greater precision, at the points marked with solid diamonds (♦), between 4% and 5% of nominal strain. Each experiment was reproduced three times on average and the obtained values of σ_y and σ_f were consistently within error margins of ±6 and ±3 MPa, respectively. The strain rate sensitivity (m), the apparent activation volume (V) and the activation energy (Q_A) of the C15 Cr_2Nb were calculated using both parameters. Fig. 3a and b presents the variation of σ_y with testing temperature and strain rate and Fig. 3c and d depicts, similarly, the corresponding variations for σ_f. It is observed that σ_y fell from ~670 MPa at 1450 °C to ~70 MPa at 1550 °C, with an apparent change in the slope close to 1400 °C; a similar behaviour is observed at $\dot{\varepsilon} > \sim 10^{-4}$ s^{-1}. Similarly, σ_f fell from ~540 MPa at 1450 °C to ~90 MPa at 1550 °C. Even though the variation *of* σ_f was relatively smoother, compared with that of σ_y, it exhibited values whose scattering from the expected behaviour was considerably larger than the experimental error. This perhaps may be due to differences in the post-yielding and steady-state flow behaviour between soft grains and hard grains and their effect in the material microstructure. More experiments would certainly produce larger and thus more faithful deviations from the expected behaviour. Alternatively, larger specimens with a wider distribution of grains and grain orientations would result in more reliable flow stress values.

If the plastic deformation of Cr_2Nb is regarded as thermally activated, then at constant T and $\dot{\varepsilon}$, the applied stress σ, the strain rate and the temperature are expected to be related to the activation energy for deformation according to the relation [17]

$$\sigma = C\dot{\varepsilon}^m e^{Q_A}/kT \tag{1}$$

for yield and steady-state flow; m is the strain rate sensitivity, Q_A the activation energy and k the Boltzmann constant. At constant temperature, Eq. (1) becomes

$$\sigma = C'(\dot{\varepsilon})^m|_T, \quad \text{or} \quad m = \left.\frac{\partial \ln \sigma}{\partial \ln \dot{\varepsilon}}\right|_{T,\varepsilon} \tag{2}$$

The regression analysis shown in Fig. 4a produced a strain rate sensitivity for yield equal to 0.27 ± 0.01, whereas for the steady-state flow the strain rate sensitivity was found equal to 0.21 ± 0.01, suggesting that the response of Cr_2Nb during yielding is more strain rate sensitive compared with steady-state flow. These modest values are typical for hot working of non-superplastic materials at temperatures of 0.5–0.8 of their melting point and lie between those for Si and Ge ($\geqslant 0.3$) and most metals and alloys ($\leqslant 0.1$). Since the stress exponent n (i.e., the inverse of the strain rate sensitivity) expresses the stress dependence of the average dislocation velocity, one might just as easily say that the initial velocity of the mobile dislocations (during yield) is less sensitive to the applied stress compared with that during steady-state flow.

The apparent activation volume (i.e., the area sheared by a dislocation during deformation) is given by the relation [18]

$$V = kT\left(\frac{\partial \ln(\dot{\varepsilon}/\dot{\varepsilon}_0)}{\partial \sigma^*}\right)\Bigg|_T \approx \frac{kT}{m\sigma^*} \tag{3}$$

where $\dot{\varepsilon}_0$ is a pre-exponential constant and σ^* is the effective stress, i.e., the applied stress minus the athermal stress, σ_a. The latter represents the resisting stress produced by long range athermal barriers to dislocation motion (e.g., dislocation tangles, forest dislocations, large incoherent precipitates and second-phase particles) which are not affected by T or $\dot{\varepsilon}$; they represent barriers too high and are thus difficult for the dislocations to surmount by thermal fluctuations. Saka et al. [9], however, performing triple strain rate cyclic compression tests on C15 Fe_2(Dy, Tb) single crystals found that σ_a is either very small or effectively zero. Similar experiments were performed in the polycrystalline Cr_2Nb at T between 1350 and 1500 °C [19]. We, therefore,

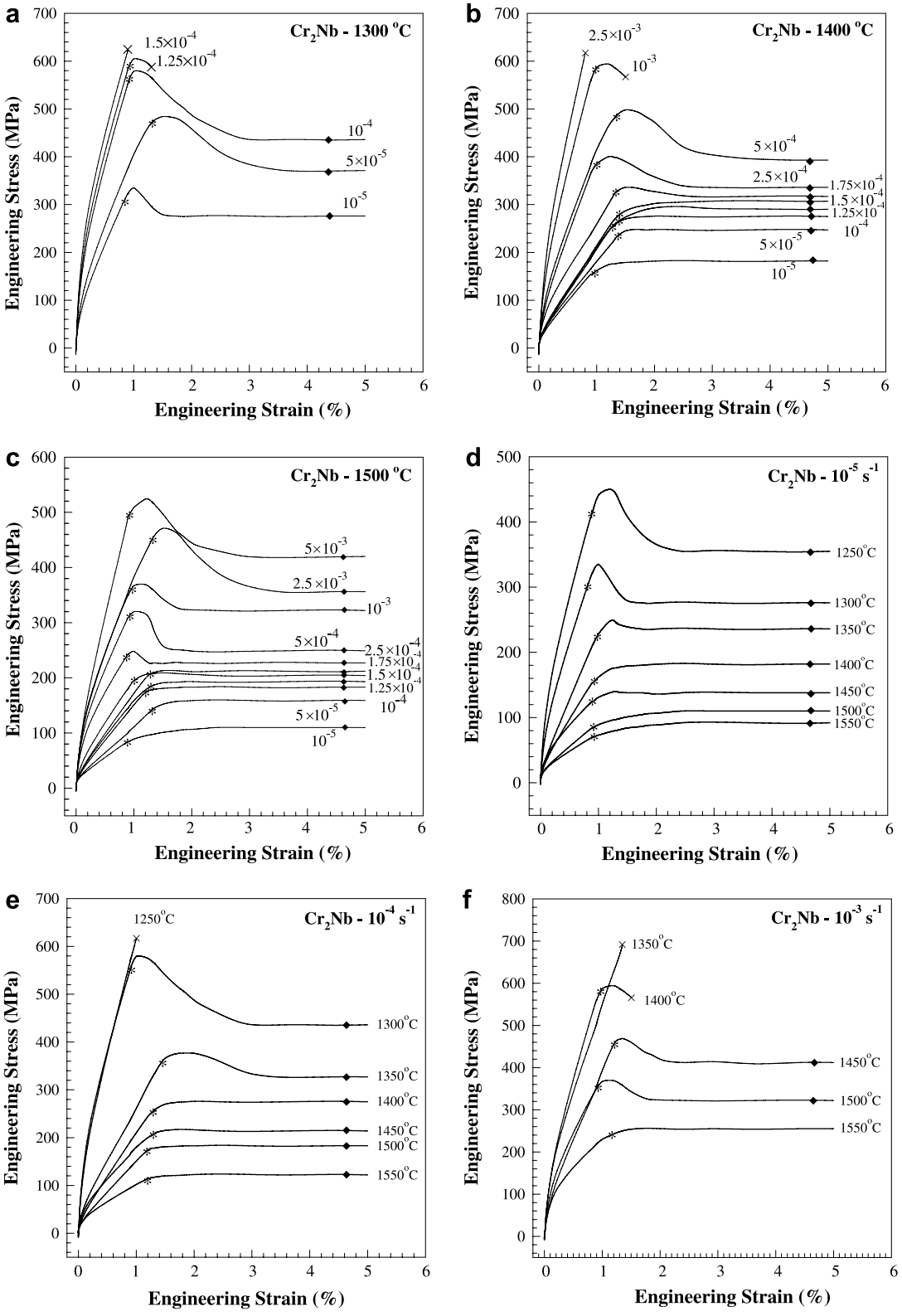

Fig. 2. Representative engineering stress–strain curves for the cubic C15 Cr_2Nb uniaxially compressed at (a) 1300 °C, (b) 1400 °C, (c) 1500 °C, (d) $\dot{\varepsilon} = 10^{-5}$ s^{-1}, (e) $\dot{\varepsilon} = 10^{-4}$ s^{-1} and (f) $\dot{\varepsilon} = 10^{-3}$ s^{-1}.

used the applied stress (i.e., σ_y and σ_f) in the last part of Eq. (3) for the calculation of the apparent activation volume (Fig. 4b). This parameter is expressed in units of $(b_{perf})^3$ and $(b_{part})^3$, where b_{perf} and b_{part} are the Burgers vectors of a perfect and a Shockley partial dislocation in the C15 Cr_2Nb ($b_{perf} = 0.4946$ and $b_{part} = 0.2856$ nm, respectively).

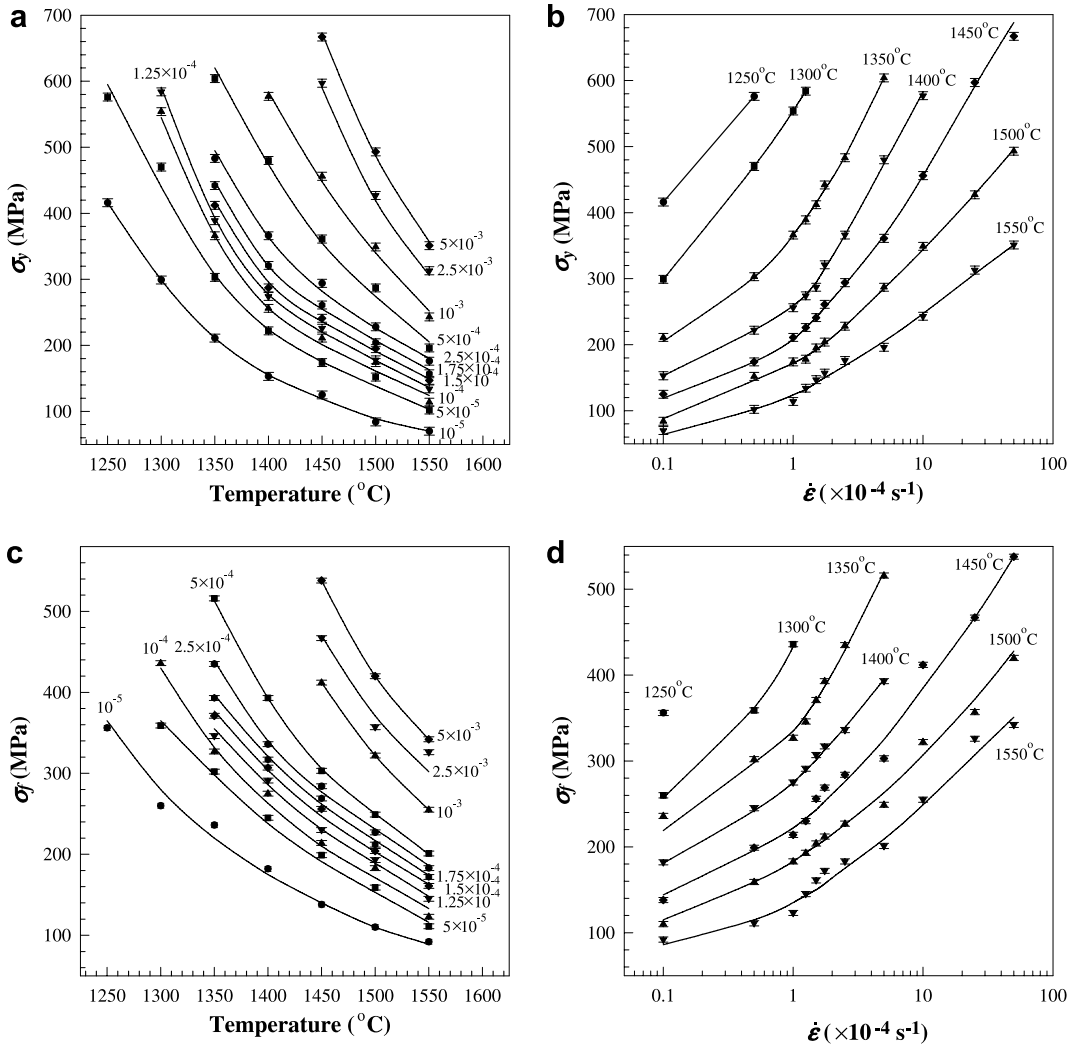

Fig. 3. (a) Variation of the yield stress with testing temperature at each strain rate; (b) variation of the yield stress with strain rate at each testing temperature; (c) variation of the flow stress with testing temperature at each strain rate; and (d) variation of the flow stress with strain rate at each testing temperature.

The variation of the apparent activation volume with the testing temperature (in units of $(b_{\text{perf}})^3$, Fig. 4c) shows that if the deformation is accomplished solely by slip, then the dislocations shear volumes ranging from 10 to slightly above 1 $(b_{\text{perf}})^3$, with decreasing temperature and increasing strain rate. These particularly small volumes are similar with those encountered in the deformation of nanocrystalline materials [20] and were comparable with those calculated by Saka et al. [9] for $V(b_{\text{perf}})^3$. For comparison, the activation volume for the bcc Nb range from 100 $(b_{\text{perf}})^3$, when σ^* approached zero to below 5 $(b_{\text{perf}})^3$ as σ^* exceeded 400 MPa [21]. Since $(b_{\text{perf}})^3$ in Cr_2Nb is approximately five times as large as that in Nb, one can easily deduce that these activation volumes may be considered comparable.

For constant strain rate, Eq. (1) becomes

$$\frac{1}{m}\ln(\sigma)\big|_{\dot{\varepsilon}} = \left.\frac{Q_A}{kT}\right|_{\dot{\varepsilon}} + C''\big|_{\dot{\varepsilon}} \tag{4}$$

where C'' is a constant. The gradients of the regression lines from plots of $\ln(\sigma)$ vs. $1/T$, at constant strain rates can deduce the variation of the Q_A for yielding and steady-state flow with (Fig. 4d). These vary from 500 kJ mol^{-1} at 10^{-5} s^{-1}, to 530 kJ mol^{-1} at 10^{-4} s^{-1}, demonstrate a local minimum at intermediate strain rates (between 1.25 and 2.5×10^{-4} s^{-1}) with a value of 450 kJ mol^{-1} at 1.5×10^{-4} s^{-1} and then increase to values >550 kJ mol^{-1} at higher. At $\dot{\varepsilon} > 10^{-3}$ s^{-1}, the consistency in the variation of Q_A between yielding and flow is lost, presumably due to changes in the microstructure which approach those of shock loading in the case of Cr_2Nb. The local minimum, however, indicates that both yielding and steady-state flow at intermediate $\dot{\varepsilon}$ may well be accomplished by a mechanism that has substantially lower demands in energy and does not rely heavily on the initial density and/or average velocity of mobile dislocations. Takasugi et al. [7] reported that single phase C15 Cr_2Nb when deformed in compression has $Q_A = 477$ kJ mol^{-1}, whereas Vignoul et al. [11] in experiments of indentation creep at 1000 and 1200 °C, deduced $Q_A = 478$ kJ mol^{-1}. These values compare very well with those deduced in this study, are larger that those

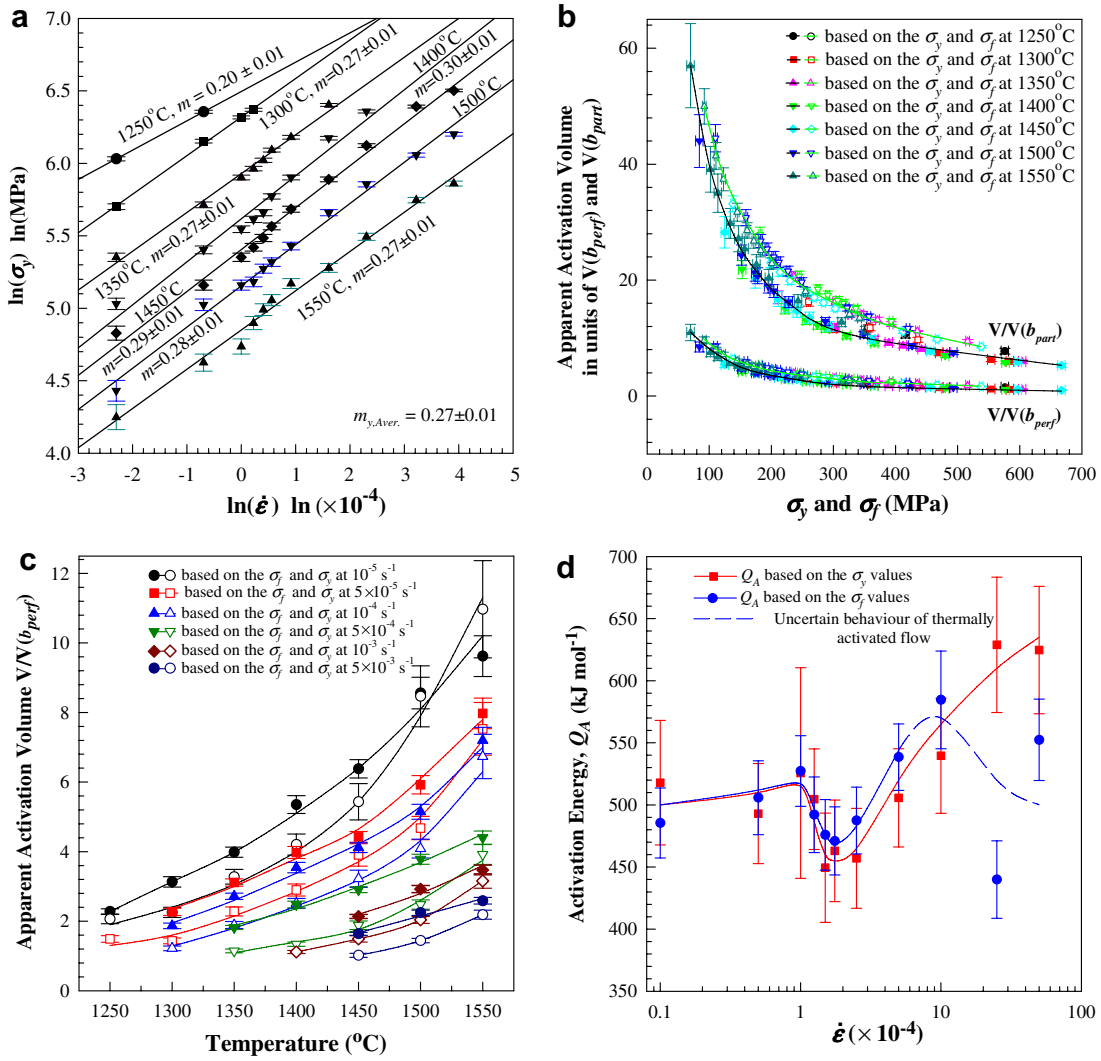

Fig. 4. (a) Linear regression plot for the calculation of the strain rate sensitivity at each testing temperature; (b) variation of the apparent activation volume with yield stress and flow stress at each testing temperature; (c) variation of the apparent activation volume with temperature at representative values of strain rate; and (d) variation of the activation energy with strain rate.

corresponding to the activation energy for self-diffusion of Nb ($Q_D = 350$ kJ mol^{-1} for vacancies and $Q_D = 440$ kJ mol^{-1} for divacancies) [22] and are very close to those corresponding to hot working of single austenitic 316 and 317 stainless steels (460 and 501 kJ mol^{-1}, respectively) [23].

3.3. Deformation microstructures

All specimens compressed at $\dot{\varepsilon} > 2.5 \times 10^{-4}$ s^{-1} or at T equal to 1300 and 1250 °C were deformed primarily by slip. At intermediate strain rates (10^{-4} s^{-1}), twins with a typical $\{1\,1\,1\}\langle 1\,1\,2\rangle$ fcc crystallography dominated the deformation microstructures. Numerous large grains were observed sheared entirely by twins formed on a single composition plane, showing always with large densities of dislocation debris at the twin boundary interface. Deformation by slip was evident on some grains but twinning was clearly dominant. At T equal to 1500 and 1550 °C, slip and twinning occurred within the same grain, whereas at lower $\dot{\varepsilon}$ and at $T < 1450$ °C most grains were deformed primarily by slip. Table 1 presents a summary of the deformation modes observed in the TEM microstructures at the temperatures and strain rates examined. Diffraction contrast analyses together with image simulations showed that slip is primarily accomplished by perfect $1/2\langle 1\,1\,0\rangle$ dislocations dissociated into pairs of Shockley partials bounding an SF. The dislocation density varied between $5 \times 10^{14} \pm 10^{14}$ m^{-2}, at $\dot{\varepsilon} = 5 \times 10^{-3}$ s^{-1} and 10^{13} m^{-2} at 10^{-4} s^{-1} and increased again at 10^{-5} s^{-1} to values close to 10^{15} m^{-2}. At high strain rates the extended dislocations seem to have a more uniform distribution, the leading partials seem to be followed closely by their trailing counterparts and largely extended intervening faults and dislocation interaction were rather rare. This behaviour is opposite to that observed in the deformation of typical fcc metals, where extensive planar fault formation is observed mostly at high strain rates. At the intermediate strain rate regime, large faults were observed and complex dislocation interactions forming

Table 1
The deformation modes in the microstructure of the C15 Cr_2Nb observed by TEM

T (°C)	Strain rate ($\dot{\varepsilon}$) ($\times 10^{-4}$ s^{-1})										
	0.1	0.5	1	1.25	1.5	1.75	2.5	5	10	25	50
1550	T		T					S			S
1500			T + S		T + S		S				
1450	S	T + S	T	T + S	S	T	S	S	S	S	S
1400			T	T	T					×	×
1350			T					×	×	×	×
1300			S	×	×	×	×	×	×	×	×
1250	S	×	×	×	×	×	×	×	×	×	×

T, twinning; S, slip; T + S, microstructures that presented equal volume fractions of twinning and slip; ×, failure of the samples prior to the completion of the test.

intrinsic/extrinsic double ribbons and three fold extended nodes (Fig. 5a), whereas at 10^{-5} s^{-1} and at 1550 °C the dislocations formed complex networks and exhibited substantial sub-boundary alignment producing sub-grains with size approximately equal to 10 μm (Fig. 5b), presumably due to creep-like deformation. At all temperatures and strain rates there was no evidence of newly formed grains (in the specimens cooled under load), whereas the possible onset of recrystallisation was observed only in a single specimen that was deformed at 1550 °C and at 10^{-4} s^{-1} and which was cooled after the load was removed. Even though the grain boundaries are not clearly observed in the optical micrograph of a specimen deformed at 1450 °C and at 1.25×10^{-4} s^{-1} (Fig. 5c), numerous traces can be seen at various orientations. These traces cannot be attributed to SFs since the specimen was electrolytically etched after polishing (i.e., the fault lines were removed). Consequently, these may only be attributed to twin boundaries and indicate the extensive deformation twinning that occurred at these testing conditions.

Diffraction contrast analyses of extended dislocations and isolated well-formed extended nodes [24], after being corrected for projection distortions and image shift [25,26] were used to calculate the SF energy, γ, by measuring the separation between the partials [27] or the local radius of curvature of the extended node [28–30]. Fig. 6 shows the variation of the shear modulus G and the SF energy with temperature. Since, there are currently no data published regarding the high temperature elastic constants of the C15 Cr_2Nb, G was calculated using the Young's modulus E (estimated by the slope of the elastic portion of the deformation curves) and the Poisson's ratio ν, equal to 0.34 [31]. The exact calculations (black curve) suggest that γ falls from 47 mJ m^{-2} at 1250 °C to ~11 mJ m^{-2} at 1550 °C. This behaviour is identical to many fcc/hcp materials as T approaches that of the fcc → hcp transformation [32]. These values are substantially lower than those calculated at 0 K from first principle calculations (116 and 94 mJ m^{-2}, for the intrinsic and extrinsic configurations, respectively [33]) and substantially larger than those previously reported (8 mJ m^{-2} at 1350 °C and 13 mJ m^{-2} at 1250 °C [13,34]). The results of the latter work, however, may well be due to calculations based on a node with edge character, or the simplicity of the formula used. A re-eval-

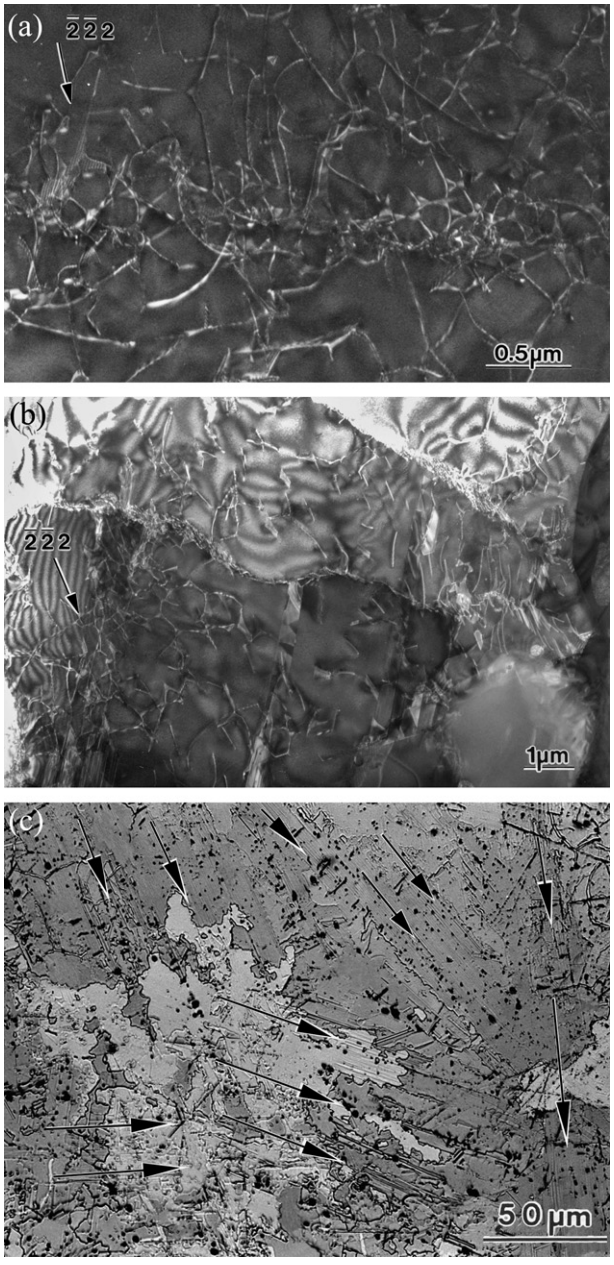

Fig. 5. (a) Extended node networks and dislocation structures (intrinsic/extrinsic ribbons) in the sample deformed at 1500 °C and at 10^{-4} s^{-1}; (b) sub-grain formation by dislocation network coalescence in the sample deformed at 1550 °C and at 10^{-5} s^{-1}; and (c) optical micrograph of a specimen compressed at 1450 °C and at 1.25×10^{-4} s^{-1}, showing twin boundary traces with various orientations.

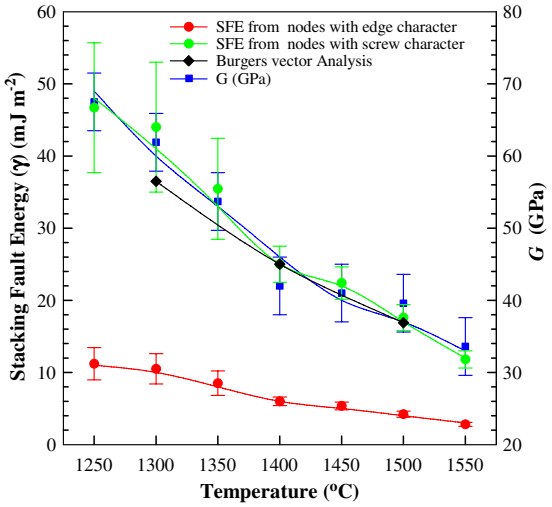

Fig. 6. Variation of the stacking fault energy of the C15 Cr_2Nb with temperature.

uation of the experimental data of Yoshida et al. [13] yielded values between 15 and 60 mJ m^{-2} (for edge and screw nodes, respectively) using the room-temperature value for G (79.6 GPa) [35], which compare very well with our present results.

Schmid factor analysis for each grain exhibiting twins was carried out by calculating the crystallographic orientation of the compression axis and estimating the angle of projection between the compression axis and the twin habit plane. Since it was not possible to differentiate between the matrix and the twin, the calculations took into account the angles between the compression axis and all six twinning directions and the highest were those attributed to the matrix. These calculations, carried out in 38 grains showing twins, showed that they could be classified into three categories.

(A) Grains of Type A (12 out of the 38) were those where the twins observed had an orientation resulting in a twinning system of the observed habit plane to have a Schmid factor higher than all other twinning and slip systems. These "primary" twins were generally isolated and did not dominate the microstructure as most grains revealed substantial dislocation between the twin bands and at the twin boundaries. According to the Schmid factor analysis, one might say that these twins were formed first and slip took over at later stages of the deformation. Their typical thicknesses were between 50 and 70 nm and the thinner they were the larger their number and/or the greater the distance between them (Fig. 7a). Primary twins were present in regions with small volume fractions between 0.05 and 0.10 with respect to the total electron transparent microstructure and in a few cases their volume fraction reached up to 0.30.

(B) Grains of type B (14 out of the 38) were those where the twins observed had an orientation resulting in a twinning system of the observed habit plane to have a Schmid factor slightly lower than that of one (eight grains) or two slip systems (six grains). The analysis showed further that in 11 out of the 14 grains, the plane of the major slip system (that with the highest Schmid factor) was the composition plane of the observed twins. It is reasonable to assume, therefore, that these twins were formed after the onset of deformation by slip (i.e., "secondary twins"). The

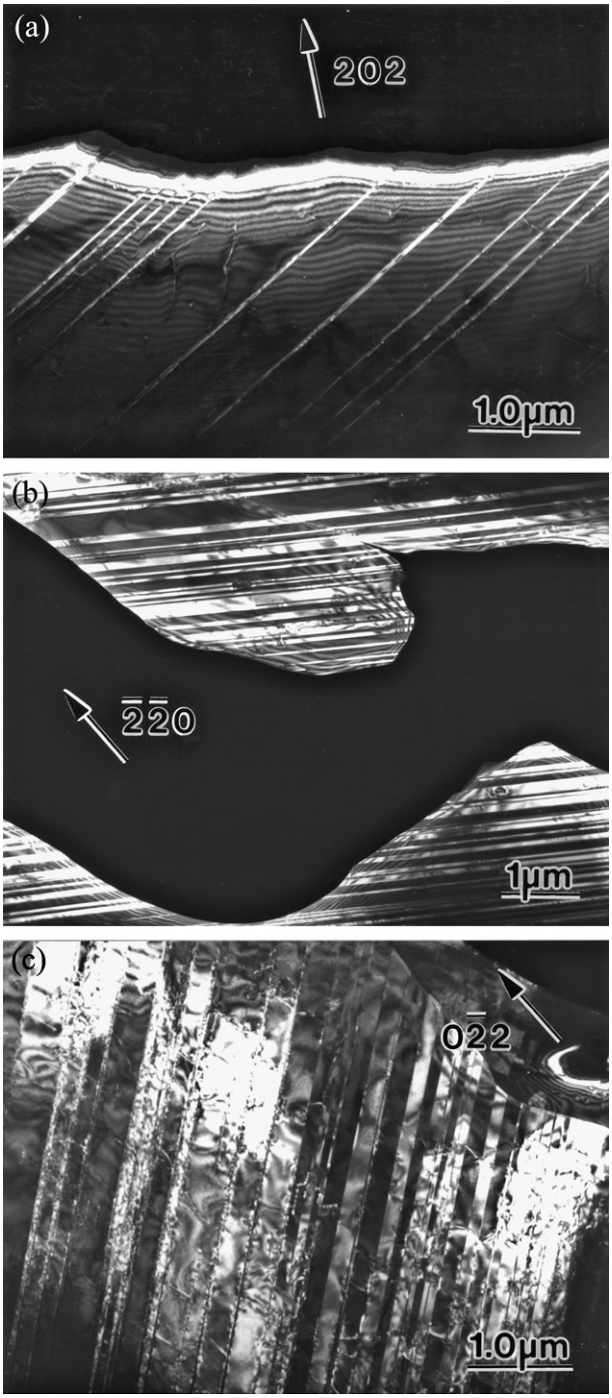

Fig. 7. (a) Twins in a grain of type A in a sample compressed at 1500 °C and at 10^{-4} s^{-1}; (b) twins in a grain of type B in a sample compressed at 1350 °C and at 10^{-4} s^{-1}; and (c) twins in a grain of type C in a sample compressed at 1450 °C and at 1.75×10^{-4} s^{-1}.

thickness of the twin bands varied between 50 and 1500 nm and their volume fraction increased as the strain rate decreased, reaching maximum values at $\dot{\varepsilon} = 10^{-4}\ s^{-1}$ and volume fractions >0.60. Interestingly, the highest volume fractions at the intermediate strain rate regime were observed when these grains were oriented so as to have two co-planar twinning systems (the major and the second major twinning system) with high and comparable Schmid factors. In these cases, the entire grain appeared twinned by successive shears (Fig. 7b).

(C) The twinning within grains of type C (12 out of the 38) could not be explained according to the Schmid factor analysis. The grain orientation was such that deformation by slip was clearly preferable; several slip systems had Schmid factors higher than those of the twinning systems and among the latter those having the higher resolved shear stresses (RSS) had composition planes different than those of the twins observed, but were apparently inactive. One would expect that these would exhibit small volume fractions, formed only to accommodate residual stresses. Nine out of the twelve grains, however, were observed heavily twinned throughout their entire microstructure. These grains were observed more frequently at intermediate strain rates, the apparently operating twinning systems had comparable Schmid factors, the twin bands had thickness varying from 50 to 300 nm and their volume fraction reached up to 0.90 (Fig. 7c).

Fig. 8 demonstrates that high RSS (for the grains of type B), but more especially comparable RSSs on two co-planar twinning systems, result in large volume fractions of twins in grains of types B and C. Twins in Laves phases have been reputed to form largely by synchroshear, i.e., two Shockley partials shearing successive triangulated "3^6" nets along two different co-planar $\langle 1\,1\,2\rangle$ orientations. The large volume fractions of the twins in grains of types B and C of the deformed C15 Cr_2Nb, therefore, indicate that when two co-planar twinning systems have high and/or comparable Schmid factors they are more likely to deform by twinning, presumably by means of the synchroshear mechanism.

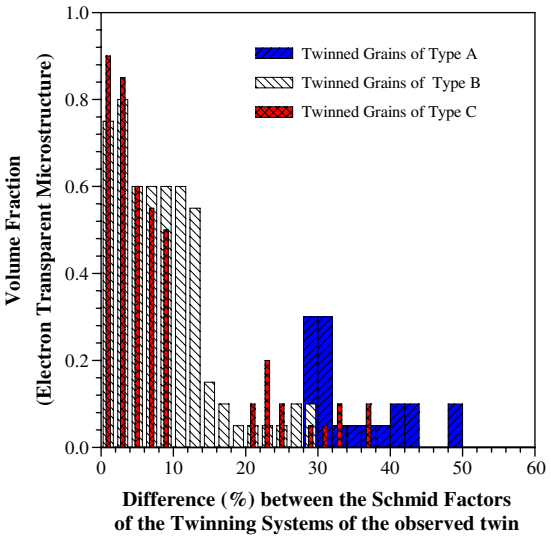

Fig. 8. Variation of the volume fraction of the twins observed in grains of types A, B and C plotted against the percentage difference between the highest Schmid factors of the twinning system responsible for producing the twins observed.

4. Discussion

The deformation microstructures demonstrate that the C15 Cr_2Nb, despite its complex crystal structure, exhibits dislocation configurations identical to those observed in many fcc materials [36,37]. There are, however, fundamental differences regarding the alloy's deformation behaviour. Common fcc metals deform by twinning at high strain rates, whereas Cr_2Nb, does so only at the intermediate strain rate regime ($<2.5\times10^{-4}\ s^{-1}$), producing particularly anisotropic microstructures with each grain showing twins on only one composition plane. By twinning, the material effectively increases the activation volume (from 1–10 $(b_{perf})^3$ to 15–60 $(b_{part})^3$) so as more effectively to accommodate the stresses imposed. The decrease in γ as T approaches that of the C15 $\rightarrow$ C14 transformation, as well as the fact that the twin band energy was calculated to be lower than γ [33] in Cr_2Nb, does not explain the observed morphology since an arbitrary deformation in a polycrystalline specimen cannot be accommodated by shears on only one composition plane. The twins in grains of type A were explained in terms of the active twinning system having the highest RSS, but they occurred irrespective of testing conditions with relatively small volume fractions (i.e., they did not dominate over slip). The twins in grains of type B, however, even though they had one or two slip systems available to carry out the deformation, showed surprisingly large volume fractions when the Schmid factor difference of the two co-planar active twinning systems was <15%. Apparently in Cr_2Nb and at these testing conditions twinning is more favourable when grains are oriented so as to have two twinning systems with high and comparable RSS. It is not unexpected for one to realize that synchroshear requires two cooperative but different $1/6\langle 1\,1\,2\rangle$ shears on the same $\{1\,1\,1\}$ plane, i.e., the simultaneous operation of two co-planar twinning systems. The passage of one synchroshockley through the major layer alters the stacking sequence of the 3^6 nets from an "αcβ-type" to an "αbγ-type" (i.e., twins the major layer) by shifting the β net of Nb atoms to the γ position, as the underlying c net of Cr atoms is shifted to the b position [38]. Evidence of the synchroshear mechanism has been recently presented [39]. Therefore, deformation by twinning may well be accomplished if the testing conditions permit the nucleation of sufficient numbers of synchroshockley partials at the grain boundaries and under the cooperative operation

of two twinning systems they shuffle across the entire grain. Twinned grains of type C had also comparable RSSs on the active twinning systems. Several slip and twinning systems, however, had larger Schmid factors. One might consider that these grains may have formerly had an orientation similar to that of type B, but that it was subsequently changed due to the strain sustained in adjoining grains. Since a 5% total strain is rather low and thus unlikely to produce such drastic changes in the surrounding microstructure, these twins can be explained only as the product of an auto-catalytic effect, in which a local stress concentration produced the first twin nucleus which in turn stimulated further nucleation and so on. Thus, a twin avalanche was produced which propagated rapidly and sheared the entire grain as observed in martensitic transformations [40]. The local minimum in the activation energy at these strain rates seems to confirm that deformation most likely does not rely so heavily on thermally activated events and, furthermore, since twinning is a strain induced transformation an auto-catalytic process may well contribute to the post-yielding softening observed for most of the specimens deformed at these strain rates and at $T < 1450$ °C.

At high $\dot{\varepsilon}$, the limited planar fault formation and the small activation volumes suggest that the dislocation motion probably encounters substantial difficulty. This difficulty prevents the leading partials from crossing large distances and despite the low γ, their trailing counterparts apparently are able to follow them. Thus the saturation of the microstructure with extended dislocations probably occurs with a rate comparable to or greater than the dislocation velocity. The fact that the deformation at high $\dot{\varepsilon}$ is a nucleation controlled process is most likely the reason for the anomalous variation of the activation energy at high strain rates, where yielding requires substantial more energy than steady-state flow. Furthermore, m_y approaches that of known semiconductors which have a low initial density of mobile dislocations. This behaviour, however, can be understood if one considers the self-pinning nature of the synchroshockley dislocations. They are immobile, unless the motion of the two Shockley partials comprising each synchroshockley occurs in a coordinated fashion so that they shear in conjunction the two adjacent 3^6 nets of the three that comprise each {1 1 1} major layer. Vacancies can facilitate synchroshear [41], but apparently their density is low and that is probably the reason the activation volume has values comparable to those of dislocation climb ($1–10b^3$), but the activation energy is much larger than that of self-diffusion. It must be emphasized that even though all the dislocations present in the TEM microstructures were dissociated, deformation by slip cannot be accomplished by the independent motion of the two synchroshockley counterparts. The expression of the activation volume in units of $(b_{perf})^3$ is due to the activation area being sheared by both components of the extended dislocations. Once the density of mobile dislocation has reached the required value, the material yields and gradually steady-state flow is established when the surplus dislocations have vacated the crystal, presumably at the grain boundaries. The stress peaks and the subsequent post-yielding softening observed in the stress–strain curves may well be explained by this process. As $\dot{\varepsilon}$ is reduced, however, the cooperative motion of the synchroshockley is more easily achieved, complex dislocation interactions may pin the leading or the trailing component of the extended dislocations and thus produce large stacking faults and complex dislocation configurations.

Previous work [7] suggested that the stress peaks and the subsequent softening observed in the stress–strain curves may be the result of dynamic recrystallisation. The deformation microstructures observed in the specimens that were cooled under load did not show any newly formed grain at the grain boundaries. Recrystallisation may well occur but at much larger strains (i.e., 20%) [34]. In addition, it was suggested that dynamic recrystallisation produced the twins observed in the microstructure, i.e., they were strain induced and this occurred due to the proximity of the testing temperature to the C14 → C15 transformation temperature. Our present results, however, showed that the largest peaks were observed mostly at high strain rates and low temperatures and at these conditions twinning was particularly limited. Furthermore, among the specimens where twinning dominated, discernible stress-peaks appeared only for those compressed at $T <$ 1450 °C, i.e., much lower than the temperature of the C14 → C15 transition. The transformation of dislocation walls into sub-boundaries can also produce softening in the stress–strain curves [42], but requires large dislocation densities, occurs at high strains ($\varepsilon > 50\%$) and the softening is achieved less swiftly compared with that observed during the compression of Cr_2Nb. The peaks in the deformation curves can only be conceived in terms of a mechanism impeding the dislocation motion, similar to strain aging of low carbon steels, where the stress-peaks at the onset of plastic deformation are associated with sites that accommodate interstitials or impurities which pin the dislocation motion. The softening prior to the establishment of steady-state flow (within nominal strain of ~2%) occurs due to an increase in the mobile dislocation density or because the dislocations managed to break away from the impurity atmosphere [43]. It has been shown, however, that deformation by slip in Laves phases is also accomplished by self-pinning synchroshockley dislocations. Since the C15 Cr_2Nb is only a weakly directional compound, its high DBTT may not be related to bonding constraints. It is probably associated with the tightly packed atomic arrangements which allow dislocation motion only when substantial softening of the crystal structure has occurred (i.e., the decrease of the elastic constants with T). The DBTT thus may correspond to the temperature where the synchroshockley dislocations are unable to overcome their self-pinning resistance so as to relieve the stress imposed and thus the material fails, most likely at the grain boundaries.

5. Conclusions

- A combination of high temperature compressions and TEM has been used to investigate the mechanical properties and the deformation microstructures of nearly stoichiometric Cr_2Nb.
- Both twinning and dislocation dissociations are related to the low γ of the C15 Cr_2Nb above the DBTT.
- Twinning dominated mostly at $10^{-4}\,s^{-1}$.
- The high volume fraction of twins within several grains could not be explained by the Schmid factor analysis and their formation on only one composition plane per grain suggested that this mechanism may be accomplished by auto-catalytic nucleation.
- Grains, however, oriented so as to have two co-planar twinning systems with high and comparable RSSs, had a higher probability to deform by twinning, in agreement with the model of twinning by the synchroshear mechanism.
- The strain rate sensitivity ($0.21 < m < 0.27$) showed that the mechanical response of the polycrystalline C15 Cr_2Nb lay between that of known semiconductors and typical fcc metals. The high m during yielding compared with that during steady-state flow was probably due to the self-pinning nature of the synchroshockleys, which probably prevented a sufficient increase in the dislocation velocity during yielding, resulting in stress-peaks similar to those shown due to strain aging of low carbon steels, especially pronounced at high $\dot{\varepsilon}$ and at low T.
- The anisotropic twinning necessitates slip to accommodate residual stresses and this is difficult unless the tightly packed structure has softened substantially and allows sufficient dislocation motion.

Acknowledgements

The authors gratefully acknowledge Professor I.R. Harris for the provision of the laboratory facilities and the EPSRC and the School of Metallurgy & Materials at the University of Birmingham, as well as the Netherlands Institute for Metals Research – Groningen for financial support (A.V.K.).

References

[1] Taub AI, Fleischer RL. Science 1989;243:616.
[2] Anton DL, Shah DM. Mater Sci Eng A 1992;153:410.
[3] Baker H, Okamoto H, Scott HD, Davidson GM, Fleming MA, Kacprzak L, et al. Binary alloy phase diagrams. ASM handbook, vol. 2. Materials Park (OH): ASM International; 1992. p. 155.
[4] Thoma DJ, Perepezko JH. Mater Sci Eng A 1992;156:97.
[5] Pope DP, Chu F. In: Darolia R, Lewandowski JJ, Liu CT, Martin PL, Mi racle DB, Nathal MV, editors. Structural intermetallics. Warrendale (PA): TMS; 1993. p. 37.
[6] Anton DL, Shah DM. In: Baker I, Darolia R, Wittenberger JD, Yoo MH, editors. High-temperature ordered intermetallic alloys V. MRS proceedings, vol. 288. Pittsburgh (PA): Materials Research Society; 1993. p. 41.
[7] Takasugi T, Hanada S, Miyamoto K. J Mater Res 1993;8:3039.
[8] Moran JB. Trans Met Soc AIME 1965;233:1473.
[9] Saka H, Hayakawa T, Nakamura M, Mizutani H, Nakamura E. Philos Mag A 1993;68:871.
[10] Ormeci A, Chu F, Wills JM, Mitchell TE, Albers RC, Thoma DJ, et al. Phys Rev B – Condens Mater 1996;54:12753.
[11] Vignoul GE, Tien JK, Sanchez JM. Mater Sci Eng A 1993;170:177.
[12] Takasugi T, Yoshida M, Hanada S. Acta Mater 1996;44:669.
[13] Yoshida M, Takasugi T, Hanada S. In: Horton J, Baker I, Hanada S, Noebe RD, editors. High-temperature ordered intermetallic alloys VI. MRS proceedings, vol. 364. Pittsburgh (PA): Materials Research Society; 1995. p. 395.
[14] Livingston JD, Hall EL. J Mater Res 1990;5:5.
[15] Liu Y, Livingston JD, Allen SM. Met Trans A 1992;23:3303.
[16] Kumar KS, Miracle DB. Intermetallics 1994;2:257.
[17] Briottet L, Jonas JJ, Montheillet F. Acta Mater 1996;44:1665.
[18] Dieter GD. Mechanical metallurgy, SI metric edition (adapted by D. Bacon). London: McGraw-Hill; 1978. p. 295.
[19] Kazantzis AV, Aindow M, Jones IP, Traintafyllidis GK, Aifantis EC, De Hosson JTM. Scr Mater, to be submitted for publication.
[20] Dao M, Lu L, Asaro RJ, Ma E, De Hosson JTM. Acta Mater 2007; accepted for publication.
[21] Taylor G. Prog Mater Sci 1992;36:29.
[22] Einziger RE, Mundy JN, Hoff HA. Phys Rev B 1978;17:440.
[23] Shi L, Northwood DO. Acta Mater 1995;43:453.
[24] Kazantzis AV, Aindow M, Jones IP. Philos Mag Lett 1996;74:129.
[25] Ruff Jr AW. Metall Trans 1970;1:2391.
[26] Cockayne DJH, Ray ILF, Whelan MJ. Philos Mag 1969;20:1265.
[27] Amelinckx S. Dislocations in particular structures. In: Nabarro FRN, editor. Dislocations in solids, vol. 2. New York (NY): North-Holland; 1979. p. 71.
[28] De Wit G, Koehler JS. Phys Rev 1959;116:1113.
[29] Brown LM, Thölén AR. Disc Faraday Soc 1964;35:37.
[30] Gallagher PCJ. J Appl Phys 1966;37:1710.
[31] Chu F, He Y, Thoma DJ, Mitchell TE. Scr Mater 1995;88:1295.
[32] Gallagher PCJ. Metall Trans 1970;1:2391.
[33] Hong S, Fu CL, Yoo MH. Philos Mag A 2000;80:871.
[34] Yoshida M, Takasugi T. Intermetallics 2002;10:85.
[35] Chu F, Ormeci AH, Mitchell TE, Wills JM, Thoma DJ, Albers RC Chen SP. Philos Mag Lett 1995;72:147.
[36] Hirth JP, Balluffi RW. Acta Mater 1973;21:929.
[37] Radetic T, Radmilovic V, Soffa WA. Scr Mater 1996;35:1403.
[38] Hazzledine PM, Pirouz P. Scr Mater 1993;28:1277.
[39] Chisholm MF, Kumar S, Hazzledine P. Science 2005;307:701.
[40] Kazantzis AV, Aindow M, Jones IP. Mater Sci Eng A 1997;233:44.
[41] Kumar KS, Hazzledine PM. Intermetallics 2004;12:763.
[42] Poschmann I, McQueen HJ. Scr Mater 1996;35:1123.
[43] Smallman RE, Bishop RJ. Metals and materials: science, processes and applications. Oxford: Butterworth–Heinemann; 1995. p. 206.